

Comparison of DSMC and particle based BGK models

## Particle-based fluid dynamics: comparison of different BGK models and DSMC for hypersonic flows

M. Pfeiffer<sup>1, a)</sup>

*Institute of Space Systems, University of Stuttgart, Pfaffenwaldring 29,  
D-70569 Stuttgart, Germany*

(Dated: 12 March 2019)

The Bhatnagar-Gross-Krook (BGK) model as well as its extensions (ellipsoidal statistical BGK, Shakhov BGK, unified BGK) are used in particle-based fluid dynamics and compared with the Direct Simulation Monte Carlo Method (DSMC). To this end, a method based on the Metropolis-Hastings algorithm is presented that allows efficient sampling of the Shakhov and the unified target distribution functions. As a consequence, particle simulations based on the Shakhov BGK and the unified BGK model are possible in an efficient way. The models are validated with a Couette flow problem at different Knudsen numbers and wall velocities. Furthermore, the models are compared with DSMC results of a hypersonic flow around a 70° blunted cone. It is shown that the unified BGK model is able to reproduce rarefied gas phenomena and the Shakhov model performs better in the reproduction of shock structures compared with the ellipsoidal statistical BGK model. Additionally, a computational time study is done to show the efficiency of BGK-based simulations for low Knudsen number flows compared with DSMC. This is especially interesting for gas flows which cover a wide range of Knudsen numbers including continuum and rarefied gas regions as in nozzle expansion flows. The fact that DSMC and the utilized BGK methods are both cell local Monte-Carlo based particle methods, makes a coupling very attractive.

Keywords: DSMC, Shakhov, Ellipsoidal statistical BGK, BGK

---

<sup>a)</sup>Electronic mail: mpfeiffer@irs.uni-stuttgart.de

## I. INTRODUCTION

Simulations of gas flows which cover a wide range of Knudsen numbers including continuum and rarefied gas regions are still challenging. CFD methods based on Navier-Stokes equations cover a wide range of near equilibrium flows that are important for many practical applications. Nevertheless, the assumptions behind the Navier-Stokes equations become invalid for rarefied non-equilibrium flows. For this purpose, the Direct Simulation Monte Carlo (DSMC) method can be used to treat non-equilibrium effects in rarefied gases. Here, discrete particle collisions are simulated for a large number of particles. Therefore, the collision integral is not solved directly. Consequently, the DSMC method becomes very expensive for small Knudsen number flows due to the fact that the mean free path as well as the collision frequency must be resolved in each collision. To close the gap between the applicable regimes of both methods, different approaches are used.

A straightforward approach to overcome this gap is the coupling of DSMC with CFD. Here, many problems arise due to the very different underlying approaches of both methods. Especially the statistical noise of the DSMC method is problematic at the boundaries between DSMC and CFD.

Another possibility to overcome this gap are particle-based continuum methods, which can be easily coupled with DSMC. A variety of different methods were introduced in the past, e.g. the Time Relaxed Monte Carlo method<sup>1</sup>, the Viscous Collision Limiter method<sup>2</sup>, the Fokker-Planck solution algorithm<sup>3,4</sup>, the low diffusion method<sup>5,6</sup> and more. A short overview with advantages and disadvantages of these methods are given in<sup>6</sup>.

Another particle method that is already used and coupled to DSMC in different applications like nozzle flow expansion<sup>7</sup>, micro channel flows (MEMS) simulations<sup>8</sup> or simulations of hypersonic shocks<sup>9</sup> is the statistical Bhatnagar-Gross-Krook (BGK) method. Up to now, only the ellipsoidal statistical BGK (ESBGK) model has been used in this context. Unfortunately, the ESBGK model does not reproduce shocks correctly<sup>10</sup>. In this publication, a method using a Metropolis-Hastings algorithm to sample in an efficient way from other target distribution functions used in the Shakhov and unified BGK models is presented. Finally, different BGK models (BGK, ESBGK, Shakhov BGK, Unified BGK) will be validated by simulating Couette flow problems and tested as well as compared concerning the reproduction of hypersonic shocks.

## II. THEORY

The Boltzmann equation fully describes the behavior of a monoatomic gas with the corresponding distribution function  $f = f(\mathbf{x}, \mathbf{v}, t)$  at position  $\mathbf{x}$  and velocity  $\mathbf{v}$

$$\frac{\partial f}{\partial t} + \mathbf{v} \frac{\partial f}{\partial \mathbf{x}} = \frac{\delta f}{\delta t} \Big|_{Coll}. \quad (1)$$

In this equation, external forces are neglected. Furthermore,  $\delta f / \delta t|_{Coll}$  is the collision term, which can be described by the Boltzmann collision integral

$$\frac{\partial f}{\partial t} \Big|_{Coll} = \int_{\mathbb{R}^3} \int_{S^2} \mathcal{B} [f(\mathbf{v}') f(\mathbf{v}'_*) - f(\mathbf{v}) f(\mathbf{v}_*)] d\mathbf{n} d\mathbf{v}_*. \quad (2)$$

Here,  $S^2 \subset \mathbb{R}^3$  is the unit sphere,  $\mathbf{n}$  is the unit vector of the scattered velocities,  $\mathcal{B}$  is the collision kernel and the superscript ' denotes the post collision velocities. The multiple integration of this collision term makes it difficult to compute in the 6D phase space.

### A. BGK Models

The BGK model approximates the collision term to a simple relaxation form where the distribution function relaxes towards a target distribution function  $f^t$  with a certain relaxation frequency  $\nu$ :

$$\frac{\partial f}{\partial t} \Big|_{Coll} = \nu (f^t - f). \quad (3)$$

The original BGK model assumes, that the target velocity distribution function is the Maxwellian velocity distribution  $f^M$

$$f^M = n \left( \frac{m}{2\pi k_B T} \right)^{3/2} \exp \left[ -\frac{m\mathbf{c}^2}{2k_B T} \right], \quad (4)$$

with the particle density  $n$ , particle mass  $m$ , temperature  $T$  and the thermal particle velocity  $\mathbf{c} = \mathbf{v} - \mathbf{u}$  from the particle velocity  $\mathbf{v}$  and the average flow velocity  $\mathbf{u}$ <sup>11</sup>. The BGK model reproduces the Maxwellian distribution in an equilibrium state, preserves conservation of mass, momentum and energy as well as fulfills the H-theorem<sup>12</sup>. The relaxation frequency  $\nu$  defines the viscosity  $\mu$  and the thermal conductivity  $K$

$$\mu = \frac{n k_B T}{\nu} \quad K = \frac{c_P n k_B T}{\nu} \quad (5)$$

with the specific heat constant  $c_P = 5k_B/2m$ . These equations clarify the problem of the BGK model concerning the Prandtl number, which is fixed in this model to  $Pr = \mu c_P / K =$

1, whereas the Prandtl number of monoatomic gases is  $Pr \approx 2/3^{12}$ . As a consequence, only the thermal conductivity or viscosity can be correctly reproduced at a time with the BGK model. To overcome this problem, several extensions of the BGK model were introduced in the past. Some of these models transform the target distribution function e.g. the ellipsoidal statistical BGK model<sup>13</sup> or the Shakhov BGK model<sup>14</sup>, other models change the relaxation frequency from a constant to a function of the microscopic velocities as described in<sup>15</sup>. In this paper, only models with a transformed target distribution are investigated.

### 1. Ellipsoidal Statistical BGK Model

The ellipsoidal statistical BGK (ESBGK) model replaces the Maxwellian target distribution of the standard BGK model with an anisotropic Gaussian distribution<sup>12</sup>

$$f^{ES} = \frac{n}{\sqrt{\det \mathcal{A}}} \left( \frac{m}{2\pi k_B T} \right)^{3/2} \exp \left[ -\frac{m \mathbf{c}^T \mathcal{A}^{-1} \mathbf{c}}{2k_B T} \right] \quad (6)$$

with the anisotropic matrix

$$\mathcal{A} = \mathcal{I} - \frac{1 - Pr}{Pr} \left( \frac{3\mathcal{P}}{\text{Tr}[\mathcal{P}]} - \mathcal{I} \right). \quad (7)$$

The anisotropic matrix  $\mathcal{A}$  consists of the identity matrix  $\mathcal{I}$  and the pressure tensor  $\mathcal{P}$

$$\mathcal{P} = \int \mathbf{c} \mathbf{c}^T f d\mathbf{v}, \quad (8)$$

which are both symmetric. The ESBGK model reproduces the Maxwellian distribution in the equilibrium state as well as the correct moments of the Boltzmann equation. Furthermore,<sup>16,17</sup> have shown that it fulfills the H-theorem. In the ESBGK model, the viscosity and the thermal conductivity are defined as

$$\mu = \frac{nk_B T}{\nu} Pr \quad K = \frac{c_P n k_B T}{\nu}. \quad (9)$$

Due to the fact that the viscosity depends on the Prandtl number, it is now possible to reproduce the viscosity and thermal conductivity at the same time. So, the introduction of the Prandtl number as an additional parameter resolves the Prandtl number problem of the standard BGK model.

As proposed by<sup>12</sup>, a symmetric transformation matrix  $\mathcal{S}$  with  $\mathcal{A} = \mathcal{S} \mathcal{S}^T$  can be defined. Furthermore, a normalized thermal velocity vector  $\mathbf{C}$  is defined such that  $\mathbf{c} = \mathcal{S} \mathbf{C}$ . Using

these definitions, the argument of the exponential function in (6) becomes

$$\mathbf{c}^T \mathcal{A}^{-1} \mathbf{c} = (\mathcal{S} \mathbf{C})^T \mathcal{S}^{-1} \mathcal{S}^{-1} \mathcal{S} \mathbf{C} = \mathbf{C}^T \mathbf{C} \quad (10)$$

using  $(\mathcal{S} \mathbf{C})^T = \mathbf{C}^T \mathcal{S}^T = \mathbf{C}^T \mathcal{S}$  due to the fact that  $\mathcal{S}$  is symmetric. So,  $\mathcal{S}$  can transform a vector  $\mathbf{C}$  sampled from a Maxwellian distribution to a vector  $\mathbf{c}$  sampled from (6).

## 2. Shakhov BGK Model

In contrast to the ESBGK model, which modifies the shear stress to produce the correct Prandtl number<sup>18</sup>, the Shakhov model (SBGK) directly modifies the heat flux. For this, the target distribution of the BGK model is changed to

$$f^S = f^M \left[ 1 + (1 - Pr) \frac{\mathbf{c} \mathbf{q}}{5(RT)^2} \left( \frac{\mathbf{c}^2}{2RT} - \frac{5}{2} \right) \right] \quad (11)$$

with the heat flux vector

$$\mathbf{q} = \int \mathbf{c} \mathbf{c}^2 f d\mathbf{v}. \quad (12)$$

In the SBGK model, the viscosity and the thermal conductivity are defined as

$$\mu = \frac{nk_B T}{\nu} \quad K = \frac{c_P n k_B T}{\nu} \frac{1}{Pr}. \quad (13)$$

Consequently, this model resolves the Prandtl number problem of the original BGK model and reproduces the Maxwellian distribution in the equilibrium state as well as the correct moments of the Boltzmann equation. The main disadvantage of the SBGK model compared to the ESBGK model is that no general proof exists whether the SBGK model always fulfills the H-theorem. Furthermore, it cannot be guaranteed that  $f^S$  is positive in each situation<sup>18</sup>.

## 3. Unified BGK Model

<sup>19</sup> proposed a unified BGK model (UBGK), which merges the ESBGK and SBGK model. The new target distribution is

$$f^U = f^{ES*} + f^{S*} \quad (14)$$

$$f^{ES*} = \frac{n}{\sqrt{\det \mathcal{A}^*}} \left( \frac{m}{2\pi k_B T} \right)^{3/2} \exp \left[ -\frac{m \mathbf{c}^T \mathcal{A}^{*-1} \mathbf{c}}{2k_B T} \right] \quad (15)$$

$$\mathcal{A}^* = \mathcal{I} + C_{ES} \left( \frac{3\mathcal{P}}{\text{Tr}[\mathcal{P}]} - \mathcal{I} \right) \quad (16)$$

$$f^{S*} = f^M (1 - C_S) \frac{\mathbf{c} \mathbf{q}}{5(RT)^2} \left( \frac{\mathbf{c}^2}{2RT} - \frac{5}{2} \right). \quad (17)$$

The UBGK model depends on two different parameters  $C_{ES}$  and  $C_S$  with

$$Pr = \frac{C_S}{1 - C_{ES}}. \quad (18)$$

Therefore, this model introduces an additional free parameter for a derived Prandtl number. This parameter can basically be chosen freely but the ES model constrains  $C_{ES}$  to the interval  $[-0.5, 1)$  to preserve positive eigenvalues of  $\mathcal{A}$ <sup>10</sup>. When  $C_{ES} = 0$  and  $C_S = Pr$  the UBGK model reduces to the Shakhov model. On the other hand, if  $C_{ES} = 1 - 1/Pr$  and  $C_S = 1$  the UBGK model is identical to the ESBGK model. For other values, the UBGK model blends the ESBGK and Shakhov model. The viscosity and the thermal conductivity for the UBGK model are defined as

$$\mu = \frac{nk_B T}{\nu(1 - C_{ES})} \quad K = \frac{c_P n k_B T}{\nu} \frac{1}{C_S}. \quad (19)$$

Finally, the UBGK model allows to modify the shear stress as well as the heat flux at once. Or with other words, the parameters  $C_{ES}$  and  $C_S$  can be used to determine different relaxation rates of  $\mathcal{P}$  and  $\mathbf{q}$ <sup>18</sup>:

$$\frac{\partial \mathcal{P}}{\partial t} = \frac{-(1 - C_{ES})}{\nu} \mathcal{P}, \quad \frac{\partial \mathbf{q}}{\partial t} = \frac{-C_S}{\nu} \mathbf{q}. \quad (20)$$

The problem of the UBGK model is that it is not clear how  $C_{ES}$  and  $C_S$  should be chosen.<sup>10</sup> exemplary show that when  $C_S$  is used to produce the right Prandtl number,  $C_{ES}$  can be derived as

$$C_{ES}^{VHS} = 1 - \frac{(7 - 2\omega)(5 - 2\omega)}{30}, \quad (21)$$

for VHS molecules with the VHS parameter  $\omega$  in an equilibrium state. Nevertheless, they also showed that  $C_{ES}$  totally differs for non-equilibrium states.

### III. IMPLEMENTATION

The different BGK models are implemented in the PIC-DSMC code PICLas<sup>20</sup> and verified by the comparison to DSMC results of PICLas. The DSMC method is widely used and details can be found in<sup>21</sup>.

For the BGK models, the statistic particle method of<sup>12,22</sup> is used. Here, particles are moved in a simulation mesh, collide with boundarys and the microscopic particle properties are sampled to calculate macroscopic values in the same manner as in DSMC. But in contrast

to the DSMC method, the collision step with binary collisions between the particles is not performed. Instead, each particle in a cell relaxes with the probability

$$P = 1 - \exp[-\nu\Delta t] \quad (22)$$

according to eq. (3) towards the target distribution. The relaxation frequency  $\nu$  is evaluated in each time step for each cell from the definition of the viscosity of each model. The relaxation frequency directly depends on the cell temperature  $T$ , which is calculated from the particle information. For the viscosity  $\mu$  the well known exponential ansatz

$$\mu = \mu_{ref} \left( \frac{T}{T_{ref}} \right)^\omega \quad (23)$$

is used. Here,  $T_{ref}$  is a reference temperature and  $\mu_{ref}$  the reference dynamic viscosity at  $T_{ref}$ <sup>7</sup>. For a VHS gas the reference dynamic viscosity can be calculated with the VHS reference diameter  $d_{ref}$  of the particles:

$$\mu_{ref} = \frac{30\sqrt{mk_B T_{ref}}}{\sqrt{\pi}4(5-2\omega)(7-2\omega)d_{ref}^2}. \quad (24)$$

If a particle is chosen to relax, the new particle velocity is sampled from the target distribution. To conserve momentum and energy, the method of<sup>12</sup> is used. For this, the average velocity and the temperature are determined before the collision ( $\mathbf{u}$  and  $T$ ) and for the postcollision conditions ( $\mathbf{u}_p$  and  $T_p$ ). The final postcollision velocity  $\mathbf{v}^*$  of every molecule (whether having undergone relaxation or not) is then determined from the provisional postcollision velocity  $\mathbf{v}_p$  according to

$$\mathbf{v}^* = \mathbf{u} + (\mathbf{v}_p - \mathbf{u}_p) \sqrt{\frac{T}{T_p}}. \quad (25)$$

## A. Relaxation Process

In the standard BGK collision term, the postcollision velocities  $\mathbf{v}_p$  are simply sampled from the Maxwellian distribution (4)

$$\mathbf{v}_p = \sigma_T, \quad (26)$$

with the normal distributed random vector  $\xi$  and the velocity  $\sigma_T = \sqrt{k_B T/m}$ .

### 1. Sampling from ESBGK

The sampling from the ESBGK distribution (6) is performed with three different approaches.

In the first approach an approximation of the transformation matrix  $\mathcal{S}$  of eq. (10) is used as described in<sup>7,9,12</sup>

$$\mathcal{S}_{ij} = \delta_{ij} - \frac{1 - Pr}{2Pr} \left[ \frac{m}{k_B T} (\mathcal{P}_{ij} - \hat{c}_i \hat{c}_j) - \delta_{ij} \right] \quad (27)$$

with

$$\hat{\mathbf{c}} = \int \mathbf{c} f d\mathbf{v}. \quad (28)$$

The advantage of this approach is that this method is fast and simple to implement. Nevertheless, the accuracy and performance of this approximation has to be tested.

The second approach is the exact calculation of  $\mathcal{S}$  by solving  $\mathcal{A} = \mathcal{S}\mathcal{S}$  to find the square root of  $\mathcal{A}$ . For this, the matrix  $\mathcal{A}$  is diagonalized to the form

$$\mathcal{A} = \mathcal{V}\mathcal{D}\mathcal{V}^T. \quad (29)$$

The columns of  $\mathcal{V}$  are the eigenvectors of  $\mathcal{A}$  and the diagonal elements of the diagonal matrix  $\mathcal{D}$  are the corresponding eigenvalues. The square root of  $\mathcal{A}$  can now be calculated with

$$\mathcal{S} = \mathcal{V}\mathcal{D}^{1/2}\mathcal{V}^T, \quad (30)$$

where the diagonal elements of the diagonal matrix  $\mathcal{D}^{1/2}$  are the square roots of the eigenvalues.

The third approach is the direct sampling from  $f^{ES}$  by using a Metropolis-Hastings method which produces a Markov chain  $\mathbf{v}_0, \mathbf{v}_1, \dots, \mathbf{v}_{N_M}$  of samples from the target distribution<sup>23–25</sup>. Starting with a sample  $\mathbf{v}_n$ , a proposed sample  $\mathbf{v}'_{n+1}$  is generated using a pre-specified density  $q(\mathbf{v}_n, \mathbf{v}'_{n+1})$  and accepted as the next sample  $\mathbf{v}_{n+1}$  of the Markov chain with the probability

$$p(\mathbf{v}_n, \mathbf{v}'_{n+1}) = \begin{cases} \min \left( 1, \frac{f(\mathbf{v}'_{n+1})q(\mathbf{v}'_{n+1}, \mathbf{v}_n)}{f(\mathbf{v}_n)q(\mathbf{v}_n, \mathbf{v}'_{n+1})} \right), & f(\mathbf{v}_n)q(\mathbf{v}_n, \mathbf{v}'_{n+1}) > 0 \\ 1, & f(\mathbf{v}_n)q(\mathbf{v}_n, \mathbf{v}'_{n+1}) = 0. \end{cases} \quad (31)$$

If the proposed value  $\mathbf{v}'_{n+1}$  is not accepted, the next step of the Markov chain is set to  $\mathbf{v}_{n+1} = \mathbf{v}_n$ . A special case of the Metropolis-Hastings method (MH) is the random-walk Metropolis

algorithm. Here,  $q$  is a symmetrical function about zero,  $q(\mathbf{v}_n, \mathbf{v}'_{n+1}) = q(\mathbf{v}'_{n+1}, \mathbf{v}_n)$  and the probability in Eq. (31) simplifies to

$$p(\mathbf{v}_n, \mathbf{v}'_{n+1}) = \min \left( 1, \frac{f(\mathbf{v}'_{n+1})}{f(\mathbf{v}_n)} \right). \quad (32)$$

For the sampling from  $f^{ES}$ ,  $q$  is chosen as a Gaussian distribution, which is symmetric. The start value of the MH algorithm is chosen with

$$\mathbf{v}_1 = \xi \quad (33)$$

and the normal distributed random vector  $\xi$ . The next proposed value is determined using a new normal distributed random vector  $\xi$ :

$$\mathbf{v}'_{n+1} = \mathbf{v}_n + \xi \quad (34)$$

A characteristic of the MH algorithm is the so called *burn-in* phase, which means that the first samples may not necessarily follow the target distribution, especially if the starting point is in a region of low density. Therefore, samples made during the *burn-in* phase have to be discarded. Different simulations have shown that 35 initial steps are sufficient to overcome the *burn-in* phase, before the first velocity is accepted. For each following final accepted velocity, the velocity should be changed at least one time and at least 10 steps in the Markov chain should be taken. Note, that the *burn-in* phase must be done in each cell every time step due to the changed target distribution.

For the ESBGK method, the probability  $p(\mathbf{v}_n, \mathbf{v}'_{n+1})$  is

$$p^{ESBGK}(\mathbf{v}_n, \mathbf{v}'_{n+1}) = \min \left( 1, \frac{\exp \left[ -0.5 \mathbf{v}'_{n+1}^T \mathcal{A}^{-1} \mathbf{v}'_{n+1} \right]}{\exp \left[ -0.5 \mathbf{v}_n^T \mathcal{A}^{-1} \mathbf{v}_n \right]} \right) \quad (35)$$

The final postcollision velocities are obtained by scaling the sampled velocities

$$\mathbf{v}_{n,p} = \mathbf{v}_n \sigma_T. \quad (36)$$

## 2. Sampling from SBGK

An analytical expression to convert a normal distributed vector in a SBGK distributed vector is not available, in contrast to the ESBGK model (see eq. (27)). Furthermore, the use of the Acceptance-Rejection method would be very inefficient due to the fact, that a 3D

vector must be sampled and the maximum of  $f^S$  must be found in each timestep. Therefore, the SBGK distribution is also sampled using the MH algorithm.

For this, exactly the same algorithm as for the ESBGK MH sampling is used, including the start and proposed velocities, the *burn-in* phase as well as the final scaling of the velocities. Only the probability in eq. (32) is changed to

$$p^{SBGK}(\mathbf{v}_n, \mathbf{v}'_{n+1}) = \min \left( 1, \frac{\exp [-0.5\mathbf{v}'_{n+1}^2] \left( 1 + (1 - Pr) \frac{\mathbf{v}'_{n+1} \mathbf{q}}{5\sigma_T^{3/2}} \left( \frac{\mathbf{v}'_{n+1}^2}{2} - \frac{5}{2} \right) \right)}{\exp [-0.5\mathbf{v}_n^2] \left( 1 + (1 - Pr) \frac{\mathbf{v}_n \mathbf{q}}{5\sigma_T^{3/2}} \left( \frac{\mathbf{v}_n^2}{2} - \frac{5}{2} \right) \right)} \right). \quad (37)$$

### 3. Sampling from UBGK

The UBGK distribution is again sampled using the MH algorithm. Like in the case of the SBGK sampling, only the probability in eq. (32) is changed

$$p^{UBGK}(\mathbf{v}_n, \mathbf{v}'_{n+1}) = \min \left( 1, \frac{\hat{p}^{UBGK,1}(\mathbf{v}'_{n+1}) + \hat{p}^{UBGK,2}(\mathbf{v}'_{n+1})}{\hat{p}^{UBGK,1}(\mathbf{v}_n) + \hat{p}^{UBGK,2}(\mathbf{v}_n)} \right), \quad (38)$$

$$\hat{p}^{UBGK,1}(\mathbf{x}) = \exp [-0.5\mathbf{x}^T \mathcal{A}^{-1} \mathbf{x}], \quad (39)$$

$$\hat{p}^{UBGK,2}(\mathbf{x}) = \exp [-0.5\mathbf{x}^2] \left( (1 - Pr) \frac{\mathbf{x} \mathbf{q}}{5\sigma_T^{3/2}} \left( \frac{\mathbf{x}^2}{2} - \frac{5}{2} \right) \right). \quad (40)$$

Note that the Metropolis-Hastings algorithm described here can basically be used to sample from an arbitrary target distribution efficiently and is not limited to the ESBGK, SBGK and the UBGK target distributions.

## IV. SIMULATION RESULTS

### A. Couette Flow

The first test case is a steady planar Couette flow of Argon similar to<sup>26</sup>. For this, two parallel plates form a channel and move in opposite directions with a velocity  $v_{Wall}$ . All other boundaries are periodic, resulting in a 1D test case. The distance between the plates is  $D = 1$  m. The simulations are performed with 100 grid cells between the plates. The DSMC solver in PICLas additionally uses an octree method<sup>27</sup>. Therefore, each cell is subdivided to resolve the mean free path of the particles. The BGK methods are performed on the same mesh but without a mesh adaptation in this test case.

| Model                               | ESBGK | ESBGK | ESBGK | SBGK           | BGK | UBGK |
|-------------------------------------|-------|-------|-------|----------------|-----|------|
|                                     | Appr. | Exact | MH    | $C_{ES} = 0.1$ |     |      |
| CPU time [s] per<br>1000 iterations | 104   | 103   | 113   | 114            | 96  | 130  |

TABLE I. CPU time of different models.

The used Argon parameters are  $d_{ref} = 4.17 \cdot 10^{-10}$  m,  $T_{ref} = 273$  K,  $\omega_{VHS} = 0.81$  and  $m = 6.631368 \cdot 10^{-26}$  kg. The initial gas temperature as well as the temperature of the plates is in each simulation  $T_{Wall} = 273$  K. Additionally, diffuse reflection with full accomodation is assumed on the plates.

### 1. Low Wall Velocity Case - $Kn \approx 0.014$

In the low velocity case, the plate velocity is  $v_{Wall} = \pm 250$  m/s and the particle density is  $n = 1.29438 \cdot 10^{20}$  1/m<sup>3</sup>. This leads to a Knudsen number of  $Kn \approx 0.014$ . The results of the temperature and velocity profiles between the plates for the different methods are shown in Fig. 1a and 1b. The ESBGK as well as the SBGK method match the DSMC results very well whereas a clear difference is visible in the temperature plot for the BGK method.

Additionally, the three different methods of sampling from the ESBGK distribution (see Sec. III A 1) are compared. Fig. 1c shows that there is no difference in the temperature plot visible. Furthermore, the computational time of the different methods is compared in Table I, showing that there is no significant difference using the different models.

### 2. High Wall Velocity Case - $Kn \approx 0.014$

The high velocity case has a plate velocity of  $v_{Wall} = \pm 750$  m/s and a particle density of  $n = 1.29438 \cdot 10^{20}$  1/m<sup>3</sup>. So, the Knudsen number is again  $Kn \approx 0.014$ . The results of this case for the temperature and velocity profiles between the plates are shown in Fig. 2a and 2b. As in the case of the low wall velocity, the ESBGK as well as the SBGK match the DSMC result very well whereas the BGK model overestimates the temperature. Furthermore, the UBGK model was tested with this case. The results compared with the DSMC method are shown in Fig. 2c and 2d. The temperature overestimates the DSMC result for the VHS

## Comparison of DSMC and particle based BGK models

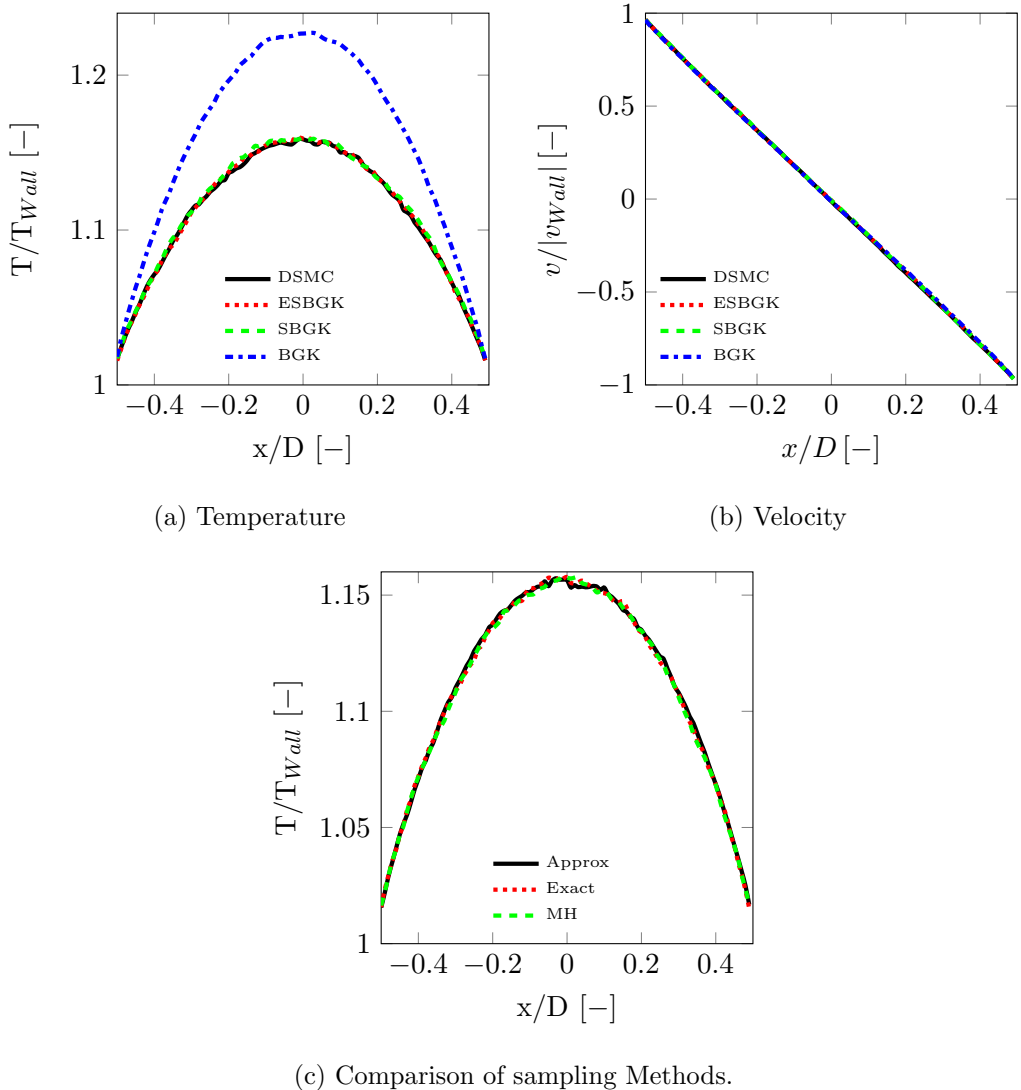


FIG. 1. a & b: Velocity and Temperature profile of low wall velocity Couette flow using different BGK models. c: Comparison of ESBGK sampling methods.

equilibrium solution of  $C_{ES} \approx 0.4$  (eq. (21)). For decreasing  $C_{ES}$ , the UBGK temperature approaches to the DSMC temperature. Clearly, the UBGK method would match the DSMC solution for  $C_{ES} = 0$  where the UBGK model reduces to the SBGK model. Nevertheless, this shows the disadvantage of the UBGK method: it is not clear how to chose the appropriate  $C_{ES}$ .

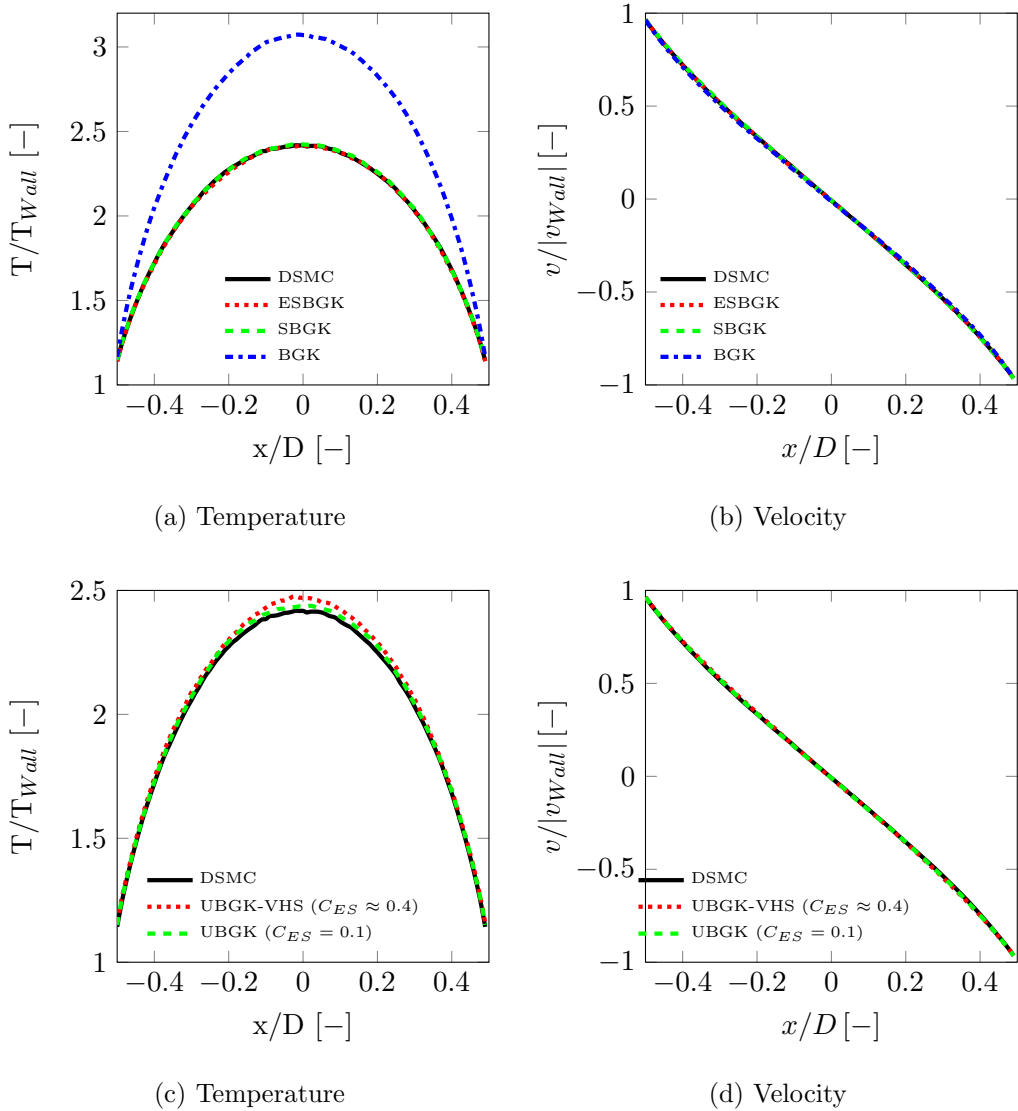


FIG. 2. a & b: Velocity and Temperature profile of high wall velocity Couette flow ( $Kn \approx 0.014$ ) using different BGK models. c & d: Velocity and Temperature profile of high wall velocity Couette flow ( $Kn \approx 0.014$ ) using the UBGK method with different  $C_{ES}$ .

### 3. High Wall Velocity Case - $Kn \approx 0.14$

The conditions are the same as described in Sec. IV A 2. The only difference is the particle density of  $n = 1.29438 \cdot 10^{19} \text{ 1/m}^3$ , which leads to a Knudsen number of  $Kn \approx 0.14$ . Therefore, this case is not in a continuum regime. The temperature and velocity profiles between the plates for the different methods are shown in Fig. 3a and 3b. Here, the SBGK method matches the DSMC results still well, whereas the BGK method overestimates and the ESBGK method underestimates the resulting temperature. Fig. 3c and 3d shows

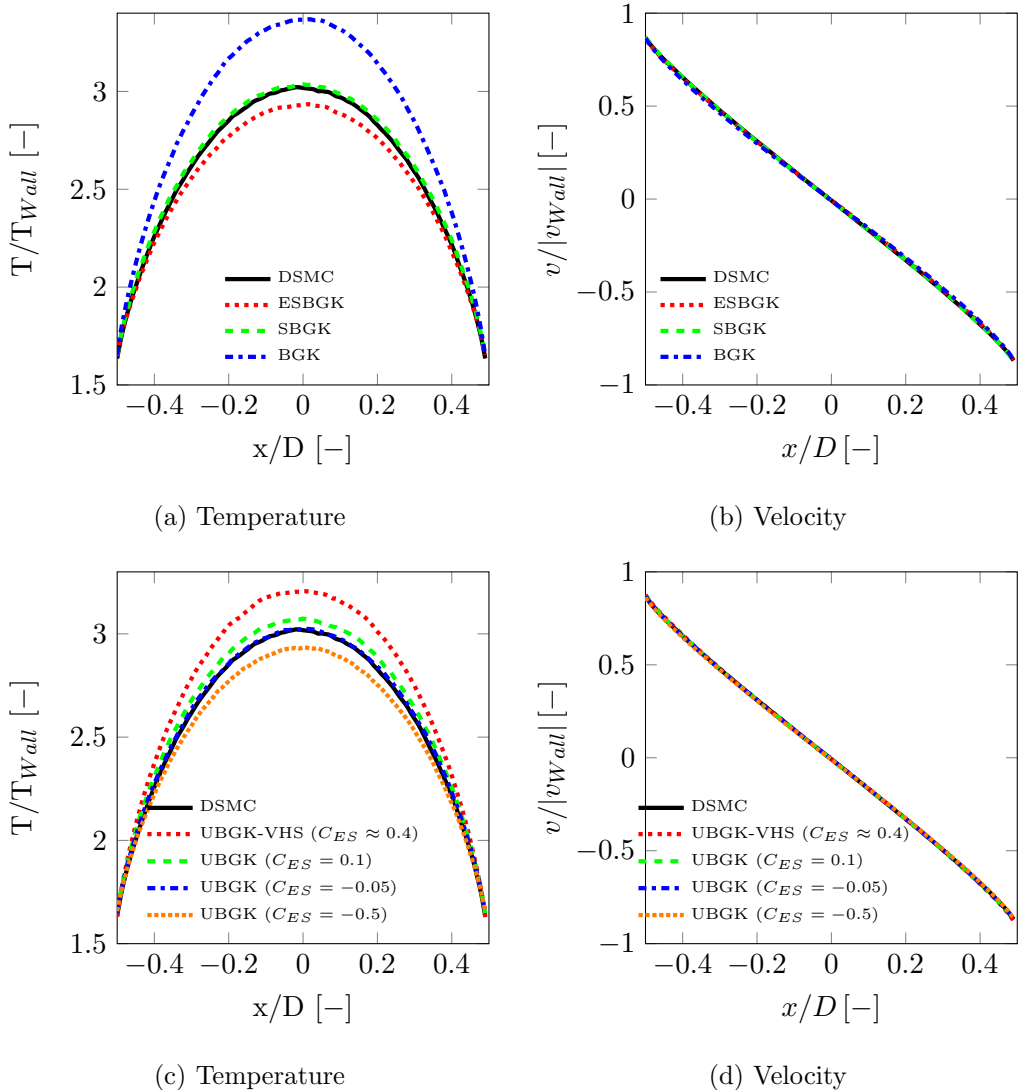


FIG. 3. a & b: Velocity and Temperature profile of high wall velocity Couette flow ( $Kn \approx 0.14$ ) using different BGK models. c & d: Velocity and Temperature profile of high wall velocity Couette flow ( $Kn \approx 0.14$ ) using the UBGK method with different  $C_{ES}$ .

additionally an advantage of the UBGK method: the UBGK results can be tuned to perfectly match the DSMC results with  $C_{ES} = -0.05$  in a non-continuum regime.

#### 4. High Wall Velocity Case - $Kn \approx 1.4$

Finally, the Knudsen number is changed to  $Kn \approx 1.4$ . In such a rarefied condition, none of the BGK methods is able to reproduce the DSMC results as shown in Fig. 4a-4d. Even the UBGK method is not capable to reproduce the correct values with the constrained

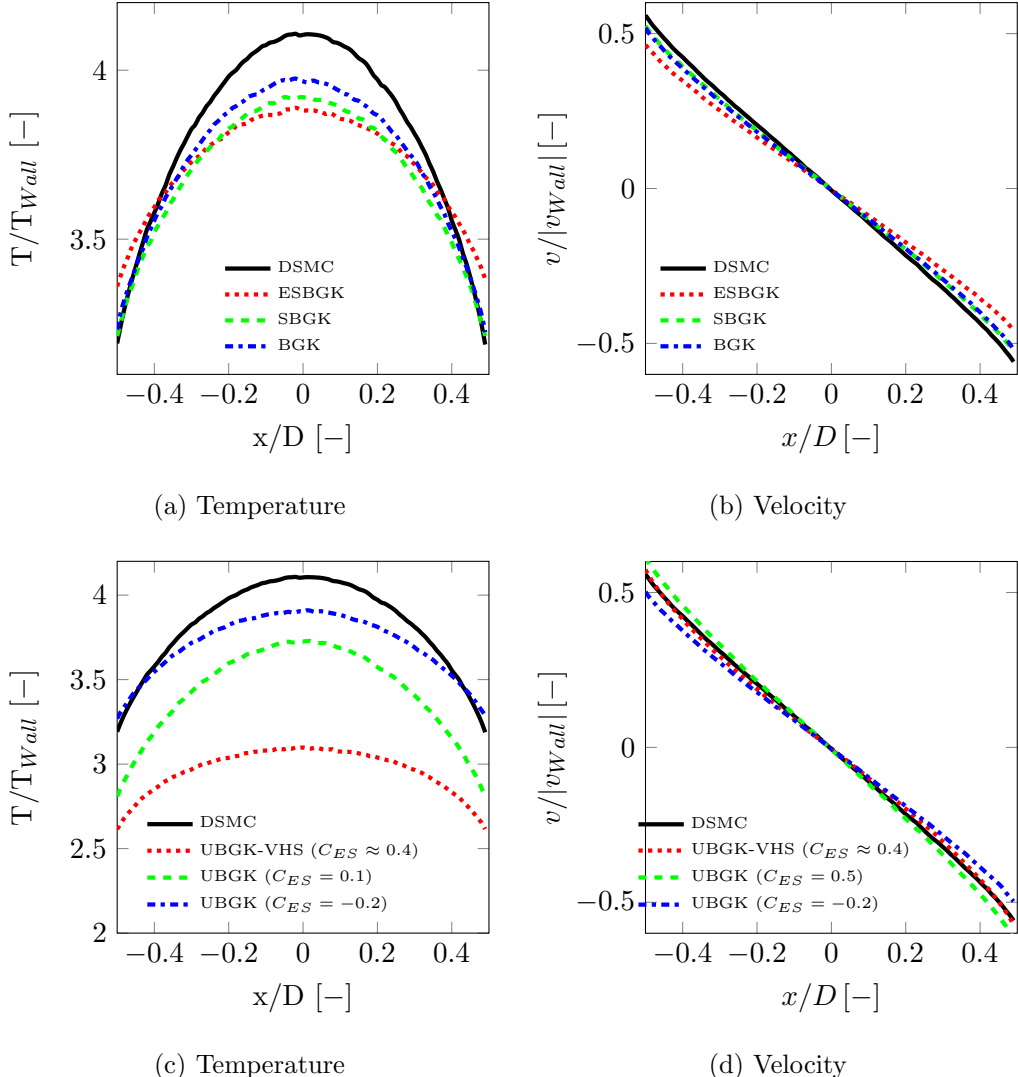


FIG. 4. a & b: Velocity and Temperature profile of high wall velocity Couette flow ( $Kn \approx 1.4$ ) using different BGK models. c & d: Velocity and Temperature profile of high wall velocity Couette flow ( $Kn \approx 1.4$ ) using the UBGK method with different  $C_{ES}$ .

$C_{ES} \in [-0.5, 1]$ .

## B. $70^\circ$ Blunted Cone

The  $70^\circ$  blunted cone described in<sup>28</sup> is chosen to compare the different BGK models with DSMC. The UBGK model was not used in this investigation. As discussed in Sec. II A 3 it is not clear how to choose  $C_{ES}$  for such complex applications. All simulations were carried out for atomic Argon with the inflow conditions of Table II.

|       | $v_\infty$ [ms $^{-1}$ ] | $T_\infty$ [K] | $n_\infty$ [m $^{-3}$ ] |
|-------|--------------------------|----------------|-------------------------|
| Set 1 | 1502.57                  | 13.3           | $3.715 \cdot 10^{20}$   |
| Set 2 | 1502.57                  | 13.3           | $1.115 \cdot 10^{21}$   |

TABLE II. Inflow conditions of 70° cone test case.

The angle of attack is set to  $\alpha = 0^\circ$ . The simulations were performed in 3D to compare the 3D performance between the BGK models and DSMC.

### 1. Set 1

Set 1 is a rarefied test case. To resolve the mean free path and the collision frequency in the 3D DSMC simulation a particle number of  $N_{DSMC} = 1.1 \cdot 10^7$  and a time step of  $\Delta t_{DSMC} = 1 \cdot 10^{-7}$  are necessary.

The BGK method has similar requirements as the CFD method. To resolve the temperature and velocity gradients a certain number of cells is required. Additionally, a certain number of particles per cell is required to represent the moments of the distribution function. Good results are obtained with at least 7 to 10 particles per cell. The timestep can be found using a classic CFL condition with the stream velocity and the speed of sound as described in<sup>6</sup>. Due to these requirements, the particle number cannot be reduced in the BGK simulations compared with the DSMC simulation for this case.

The comparison of the heat flux and force in x-direction between the different methods is shown in Fig. 5a and 5b. The Points {A,B,C,D} in Fig. 5a and 5b correspond with the points depicted in Fig. 8a. The SBGK as well as the ESBGK model match the DSMC results very well, whereas the pure BGK model underestimates the heat flux. Fig. 5c shows the temperature plot over the stagnation stream line. While the SBGK model agrees well with the DSMC result, the ESBGK model shows a well-known problem. It predicts an early onset of the temperature increase, which results in wider temperature profiles in shock waves<sup>9,10</sup>.

Furthermore, a discretization study was done for the SBGK model because it best reproduces the shock profile as well as the heat flux. For this purpose, the simulation was performed with different timestep sizes. The results concerning the heat flux and the shock

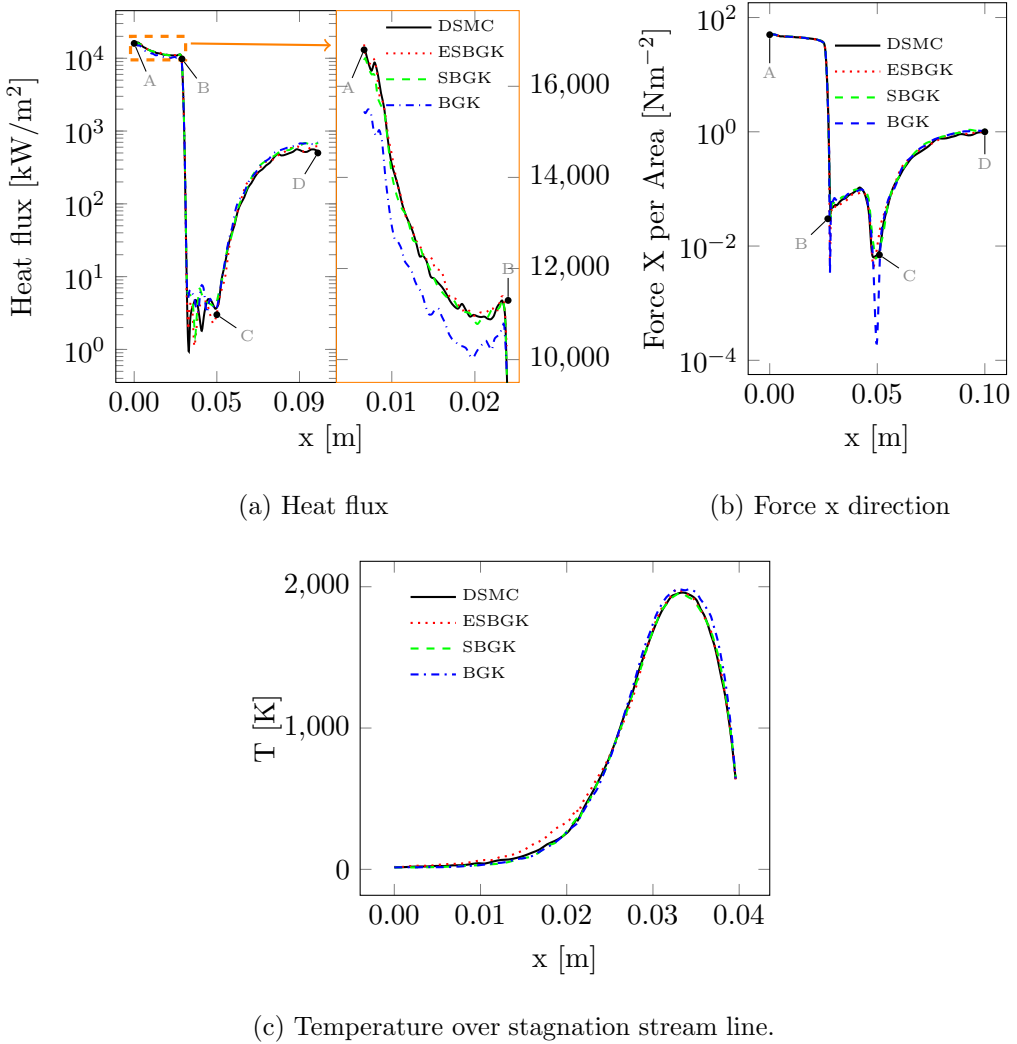


FIG. 5. Cone Set 1. a: Heatflux plot with magnification of the shield front region. b: Force on shield in x direction. The points  $\{A,B,C,D\}$  correspond to the points depicted in Fig. 8a. c: Comparison of the temperature (shock structure) plot over the stagnation stream line between different models. Particle number and timestep for DSMC:  $N_{DSMC} = 1.1 \cdot 10^7$ ,  $\Delta t_{DSMC} = 1 \cdot 10^{-7}$ . Particle number and timestep for the BGK models:  $N = N_{DSMC}$ ,  $\Delta t = \Delta t_{DSMC}$ .

structure of this investigation are shown in Fig. 6a and 6b. The heat flux and the shock structure match the DSMC results well up to  $\Delta t = 2\Delta t_{DSMC}$ .

A comparison of the computational time is shown in Table III. As expected, the needed CPU time is similar for all methods due to the same needed discretization.

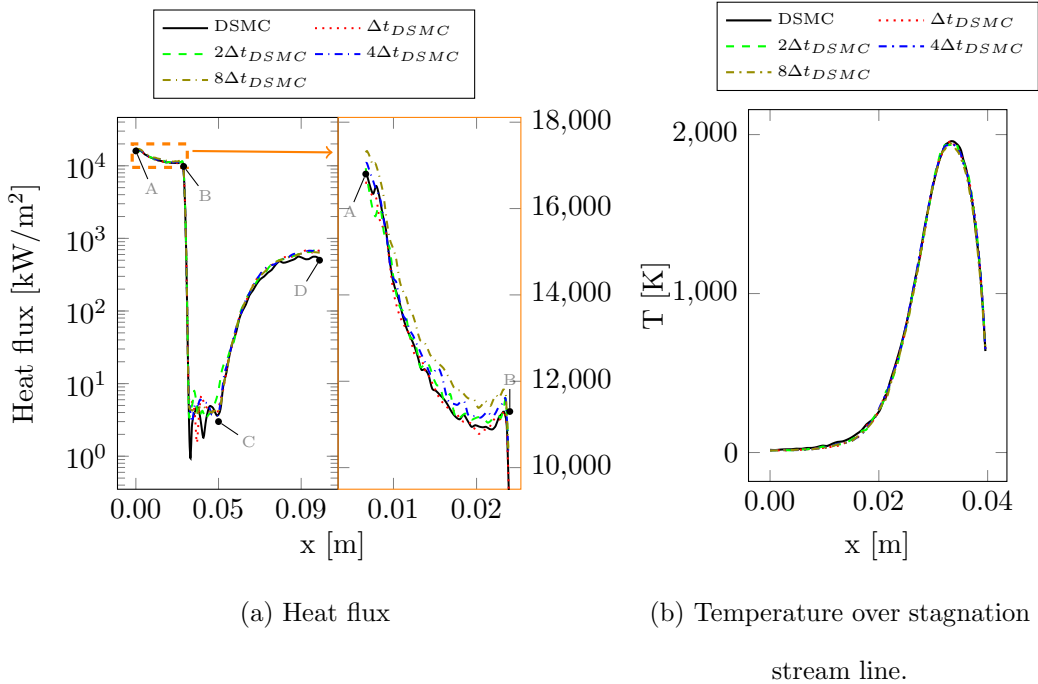


FIG. 6. Comparison of the heat flux and temperature plot over the stagnation stream line between different time step discretizations using SBGK.

|       | Particle         | Timestep            | CPU Time / 100 | CPU Time / $1 \cdot 10^{-5}$ s |
|-------|------------------|---------------------|----------------|--------------------------------|
|       | Number $N$       | $\Delta t$          | iterations [s] | Simulation time [s]            |
| DSMC  | $1.1 \cdot 10^7$ | $1 \cdot 10^{-7}$ s | 330            | 660                            |
| ESBGK | $N_{DSMC}$       | $\Delta t_{DSMC}$   | 300            | 600                            |
| SBGK  | $N_{DSMC}$       | $\Delta t_{DSMC}$   | 330            | 660                            |
| BGK   | $N_{DSMC}$       | $\Delta t_{DSMC}$   | 300            | 600                            |
| SBGK  | $N_{DSMC}$       | $2\Delta t_{DSMC}$  | 400            | 400                            |

TABLE III. Comparison of CPU time between the different methods for Set 1.

## 2. Set 2

The conditions of Set 2 are given in Table II, where a higher density is assumed. To resolve the mean free path as well as the collision frequency in the 3D DSMC simulation a particle number of  $N_{DSMC} = 5.4 \cdot 10^7$  and a time step of  $\Delta t_{DSMC} = 5 \cdot 10^{-8}$  are necessary. The comparison of the heat flux and force in x-direction between the different methods is

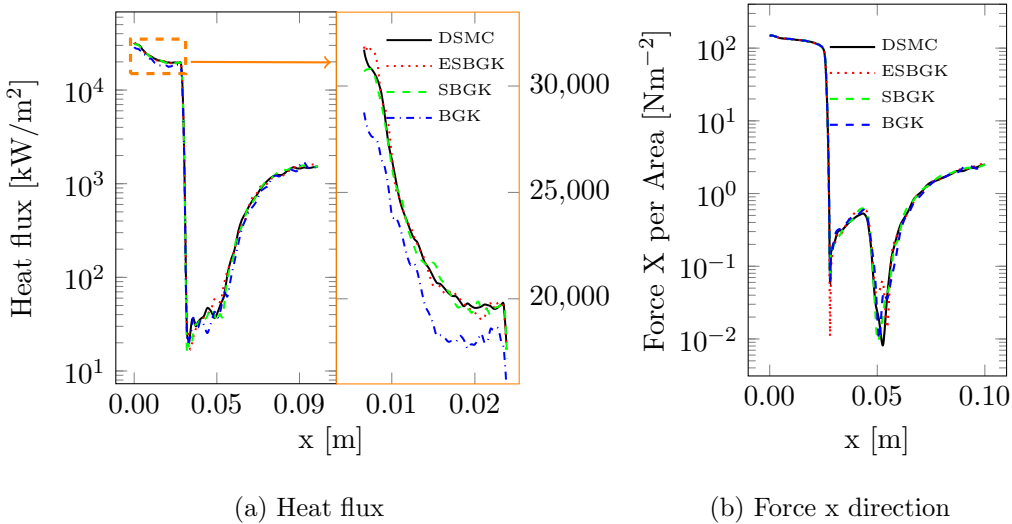


FIG. 7. Comparison of DSMC with the different BGK models. Particle number and timestep for DSMC:  $N_{DSMC} = 5.4 \cdot 10^7$ ,  $\Delta t_{DSMC} = 5 \cdot 10^{-8}$ . Particle number and timestep for the BGK models:  $N = N_{DSMC}/4$ ,  $\Delta t = 2\Delta t_{DSMC}$ .

shown in Fig. 7a and 7b. Here, all simulations with the different BGK models are performed with four times less particles  $N = N_{DSMC}/4$  and a two times larger timestep  $\Delta t = 2\Delta t_{DSMC}$ . Again, the SBGK as well as the ESBGK model match the DSMC results very well, whereas the pure BGK model underestimates the heat flux. Once more, the SBGK model shows the best agreement with DSMC between the BGK-based models in terms of the shock structure as shown in Fig. 8a and 8b and in more detail in Fig. 9a.

Also a discretization study was done with the SBGK model for this test case. For this purpose, the simulation was performed with different timestep sizes and particle numbers. The results concerning the shock structure of this investigation is also shown in fig. 9b. The SBGK results in terms of the shock structure matches the DSMC result better with increasing discretization but the shock structure is still acceptable with  $N = N_{DSMC}/8$  and  $\Delta t = 4\Delta t_{DSMC}$ . For the heat flux, the  $N = N_{DSMC}/8$  and  $\Delta t = 4\Delta t_{DSMC}$  case overestimates the DSMC result as shown in Fig. 10. However, good agreement in heat flux and shock structure are achieved with  $N = N_{DSMC}/8$  and  $\Delta t = 2\Delta t_{DSMC}$ .

A comparison of the CPU time is depicted in Table IV. In this case, the BGK methods can save computational time compared with DSMC. For the coarsest discretization with acceptable results in terms of the heat flux and shock structure ( $N = N_{DSMC}/8$ ,  $\Delta t = 2\Delta t_{DSMC}$ ) the SBGK model reduces the CPU time by a factor of  $\approx 17.5$  to reach the same

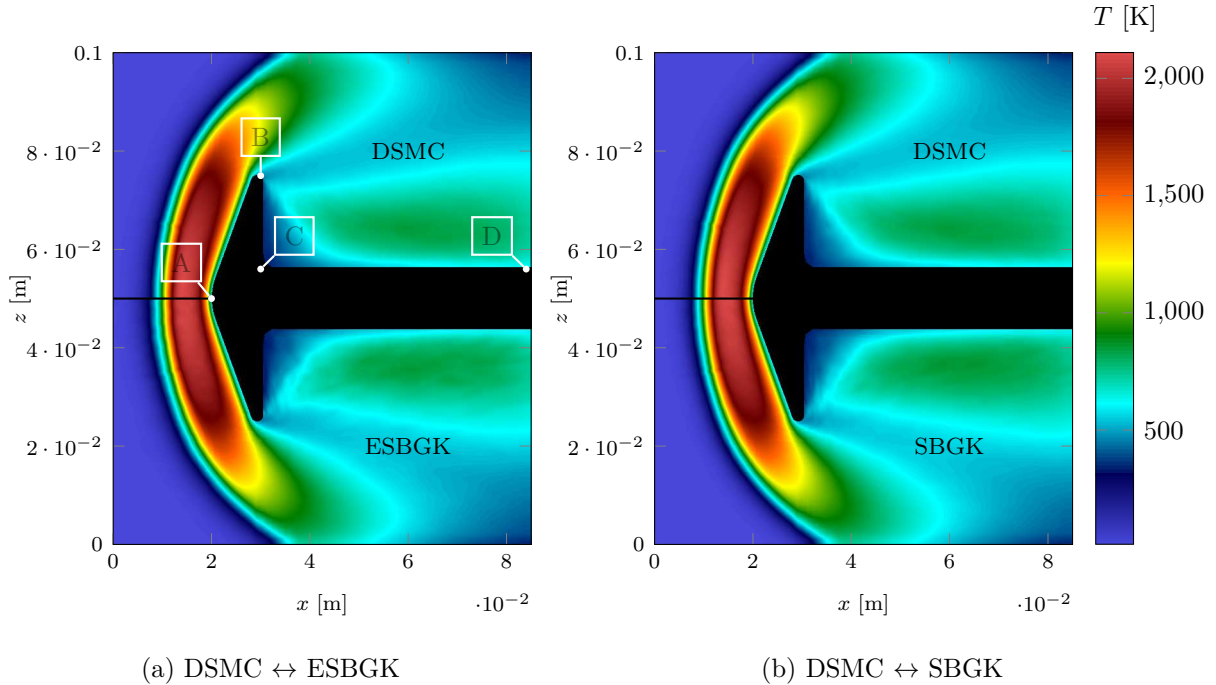


FIG. 8. Temperature plots of ESBGK, SBGK and DSMC to compare the shock structure.

|       | Particle         | Timestep            | CPU Time / 100 | CPU Time / $1 \cdot 10^{-5}$ s |
|-------|------------------|---------------------|----------------|--------------------------------|
|       | Number $N$       | $\Delta t$          | iterations [s] | Simulation time [s]            |
| DSMC  | $5.4 \cdot 10^7$ | $5 \cdot 10^{-8}$ s | 2820           | 5630                           |
| ESBGK | $N_{DSMC}/4$     | $2\Delta t_{DSMC}$  | 480            | 480                            |
| SBGK  | $N_{DSMC}/4$     | $2\Delta t_{DSMC}$  | 580            | 580                            |
| BGK   | $N_{DSMC}/4$     | $2\Delta t_{DSMC}$  | 480            | 480                            |
| SBGK  | $N_{DSMC}/8$     | $2\Delta t_{DSMC}$  | 320            | 320                            |

TABLE IV. Comparison of CPU time between the different methods for Set 2.

simulation time.

## V. CONCLUSION

An efficient method based on the Metropolis-Hastings algorithm to sample a 3D vector from an arbitrary velocity distribution function was proposed. Using this method, it was possible to use the Shakhov BGK and the unified BGK models in an efficient way in the

## Comparison of DSMC and particle based BGK models

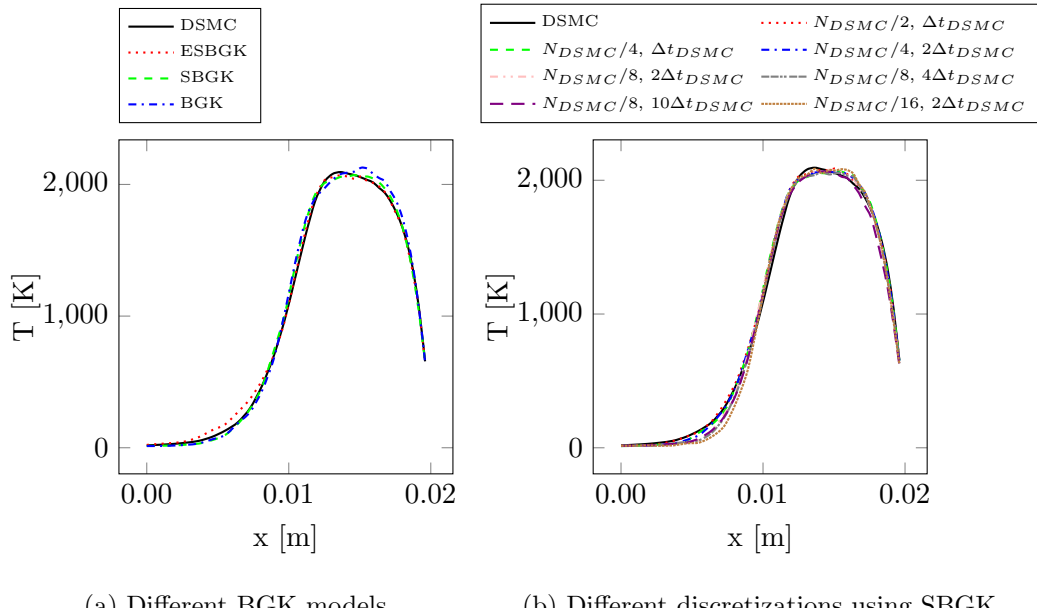


FIG. 9. Comparison of the temperature plot over the stagnation stream line between different models and discretizations.

context of particle simulations.

The new method was validated using Couette flow test cases with different wall velocities and Knudsen numbers. It was shown that the SBGK model performs well up to  $Kn = 0.14$  whereas the ESBGK model shows distinct differences to the DSMC simulations in this Knudsen number regime. Furthermore, it was demonstrated that it is possible to capture rarefied flow phenomena using the UBGK model by adapting the additional free parameter of the UBGK model. Nevertheless, it is currently not clear how this additional free parameter should be defined. Therefore, the UBGK model is not useful for practical applications at the moment. Additionally, the computational time of the different BGK methods were compared. Here, it was shown that the introduced Metropolis-Hastings based algorithm is not significantly slower than the established method to sample from the ESBGK target function and enables the sampling from the SBGK and UBGK target distribution in an efficient applicable way.

Further on, the BGK, SBGK and ESBGK model were compared with DSMC simulations based on the hypersonic flow around a  $70^\circ$  blunted cone to evaluate the capabilities to capture shock waves. As expected, the shock profile was best reproduced by the SBGK model. However, the heat flux of the SBGK as well as the ESBGK model match the DSMC

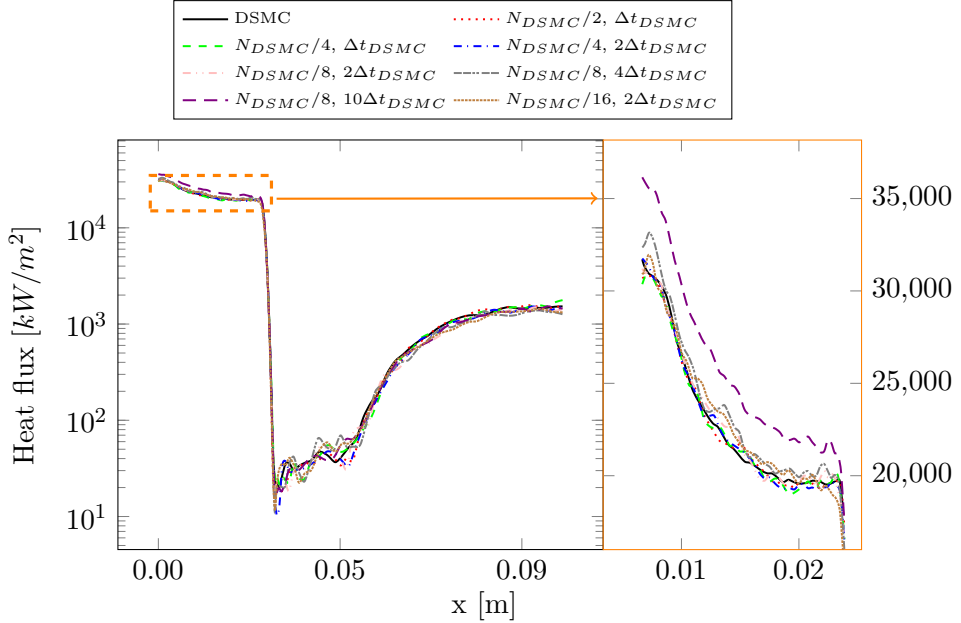


FIG. 10. Comparison of heat flux between DSMC and the SBGK model with different discretizations.

result very well. It was shown that for a low density case (Case 1), the CPU time for DSMC and the BGK models were nearly the same. With increasing density, the BGK models are able to save significant CPU time compared with DSMC. It was demonstrated that the SBGK model can save up to a factor of  $\approx 17.5$  CPU time compared with DSMC.

This behavior is especially very interesting for gas flows which cover a wide range of Knudsen numbers including continuum and rarefied gas regions as in nozzle expansion flows, where the coupling of the proposed BGK methods with DSMC is required in order to save computational time. The fact that DSMC and the investigated methods are both cell local Monte-Carlo based particle methods, makes a coupling very simple without the typical problems of hybrid CFD-DSMC methods.

## ACKNOWLEDGMENTS

The author gratefully acknowledges the Deutsche Forschungsgemeinschaft (DFG) for funding this research within the project “Partikelverfahren mit Strahlungslöser zur Simulation hochenthalper Nichtgleichgewichts-Plasmen” (project number 93159129). The author also thanks the High Performance Computing Center Stuttgart (HLRS) for granting the

computational time that has allowed the execution of the presented simulations.

## REFERENCES

<sup>1</sup>L. Pareschi and S. Trazzi, “Numerical solution of the Boltzmann equation by time relaxed Monte Carlo (TRMC) methods,” *International Journal for Numerical Methods in Fluids* **48**, 947–983 (2005).

<sup>2</sup>D. S. Liechty and J. M. Burt, “Extension of the viscous collision limiting direct simulation Monte Carlo technique to multiple species,” in *AIP Conference Proceedings* (2016) p. 050008.

<sup>3</sup>M. H. Gorji and P. Jenny, “An efficient particle FokkerPlanck algorithm for rarefied gas flows,” *Journal of Computational Physics* **262**, 325–343 (2014).

<sup>4</sup>M. Pfeiffer and M. Gorji, “Adaptive particlecell algorithm for fokkerplanck based rarefied gas flow simulations,” *Computer Physics Communications* **213**, 1 – 8 (2017).

<sup>5</sup>J. M. Burt and I. D. Boyd, “A low diffusion particle method for simulating compressible inviscid flows,” *Journal of Computational Physics* **227**, 4653–4670 (2008).

<sup>6</sup>A. Mirza, P. Nizenkov, M. Pfeiffer, and S. Fasoulas, “Three-dimensional implementation of the low diffusion method for continuum flow simulations,” *Computer Physics Communications* **220**, 269 – 278 (2017).

<sup>7</sup>J. Burt and I. Boyd, “Evaluation of a particle method for the ellipsoidal statistical bhatnagar-gross-krook equation,” in *44th AIAA Aerospace Sciences Meeting and Exhibit* (2006) p. 989.

<sup>8</sup>E. Titov, R. Kumar, D. Levin, N. Gimelshein, and S. Gimelshein, “Analysis of different approaches to modeling of nozzle flows in the near continuum regime,” in *AIP Conference Proceedings*, Vol. 1084 (AIP, 2008) pp. 978–984.

<sup>9</sup>O. Tumuklu, Z. Li, and D. A. Levin, “Particle ellipsoidal statistical bhatnagar–gross–krook approach for simulation of hypersonic shocks,” *AIAA Journal* , 3701–3716 (2016).

<sup>10</sup>S. Chen, K. Xu, and Q. Cai, “A comparison and unification of ellipsoidal statistical and shakhov bgk models,” *Advances in Applied Mathematics and Mechanics* **7**, 245–266 (2015).

<sup>11</sup>P. L. Bhatnagar, E. P. Gross, and M. Krook, “A model for collision processes in gases. i. small amplitude processes in charged and neutral one-component systems,” *Physical review* **94**, 511 (1954).

<sup>12</sup>M. Gallis and J. Torczynski, “Investigation of the ellipsoidal-statistical bhatnagar–gross–krook kinetic model applied to gas-phase transport of heat and tangential momentum between parallel walls,” *Physics of Fluids* **23**, 030601 (2011).

<sup>13</sup>L. H. Holway Jr, “New statistical models for kinetic theory: methods of construction,” *The Physics of Fluids* **9**, 1658–1673 (1966).

<sup>14</sup>E. Shakhov, “Generalization of the krook kinetic relaxation equation,” *Fluid Dynamics* **3**, 95–96 (1968).

<sup>15</sup>H. Struchtrup, “The bgk-model with velocity-dependent collision frequency,” *Continuum Mechanics and Thermodynamics* **9**, 23–31 (1997).

<sup>16</sup>P. Andries, P. Le Tallec, J.-P. Perlat, and B. Perthame, “The gaussian-bgk model of boltzmann equation with small prandtl number,” *European Journal of Mechanics-B/Fluids* **19**, 813–830 (2000).

<sup>17</sup>P. Andries and B. Perthame, “The es-bgk model equation with correct prandtl number,” in *AIP conference proceedings*, Vol. 585 (AIP, 2001) pp. 30–36.

<sup>18</sup>X. Kun, *Direct modeling for computational fluid dynamics: construction and application of unified gas-kinetic schemes*, Vol. 4 (World Scientific, 2014).

<sup>19</sup>K. Xu and J.-C. Huang, “A unified gas-kinetic scheme for continuum and rarefied flows,” *Journal of Computational Physics* **229**, 7747–7764 (2010).

<sup>20</sup>C.-D. Munz, M. Auweter-Kurtz, S. Fasoulas, A. Mirza, P. Ortwein, M. Pfeiffer, and T. Stindl, “Coupled Particle-In-Cell and Direct Simulation Monte Carlo method for simulating reactive plasma flows,” *Comptes Rendus Mécanique* **342**, 662–670 (2014).

<sup>21</sup>G. A. Bird, *Molecular Gas Dynamics and the Direct Simulation of Gas Flows*, 2nd ed. (Oxford University Press, New York, 1994).

<sup>22</sup>M. Gallis and J. Torczynski, “The application of the bgk model in particle simulations,” in *34th Thermophysics Conference* (2000) p. 2360.

<sup>23</sup>S. Chib and E. Greenberg, “Understanding the metropolis-hastings algorithm,” *The American Statistician* **49**, pp. 327–335 (1995).

<sup>24</sup>W. K. Hastings, “Monte carlo sampling methods using markov chains and their applications,” *Biometrika* **57**, 97–109 (1970).

<sup>25</sup>M. Pfeiffer, P. Nizenkov, A. Mirza, and S. Fasoulas, “Direct simulation monte carlo modeling of relaxation processes in polyatomic gases,” *Physics of Fluids* **28**, 027103 (2016).

## Comparison of DSMC and particle based BGK models

<sup>26</sup>R. Kumar, E. Titov, and D. Levin, “Comparison of statistical bgk and dsmc methods with theoretical solutions for two classical fluid flow problems,” in *41st AIAA Thermophysics Conference* (2009) p. 3740.

<sup>27</sup>M. Pfeiffer, A. Mirza, and S. Fasoulas, “A grid-independent particle pairing strategy for DSMC,” *Journal of Computational Physics* **246**, 28–36 (2013).

<sup>28</sup>J. Allègre, D. Bisch, and J. C. Lengrand, “Experimental Rarefied Heat Transfer at Hypersonic Conditions over 70-Degree Blunted Cone,” *Journal of Spacecraft and Rockets* **34**, 724–728 (1997).